



## Surface complexation and dissolution of hematite by C<sub>1</sub>-C<sub>6</sub> dicarboxylic acids at pH = 5.0

OWEN W. DUCKWORTH and SCOT T. MARTIN\*

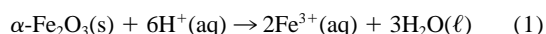
Division of Engineering and Applied Sciences, Pierce Hall, 29 Oxford St., Harvard University, Cambridge, MA 02138, USA

(Received January 31, 2001; accepted in revised form May 14, 2001)

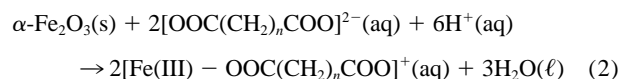
**Abstract**—Adsorption of organic ligands to the surfaces of minerals is a ubiquitous environmental process that often regulates interfacial aqueous chemistry. In the current work, the infrared spectra of dicarboxylate ligands adsorbed to hematite are collected by attenuated total reflectance (ATR) spectroscopy. For each ligand, spectra are recorded at several concentrations at pH = 5.0. Each series of spectra is analyzed by singular value decomposition constrained to a Langmuir adsorption surface model. Oxalate, malonate, and glutarate form bidentate surface complexation structures, whereas succinate and adipate form monodentate structures. The absence of a linear trend in the qualitative form of the binding structure (e.g., bidentate for  $n = 0, 1,$  and  $3$  and monodentate for  $n = 2$  and  $4$  where  $n$  is the length of the carbon chain between carboxylate groups) is attributed to the variation of strain energies for the geometries of possible surface complexation structures. For the bidentate ligands, a linear relationship between the Langmuir binding constant and the second acidity constant is demonstrated. The ligand-promoted dissolution rates at pH = 5.0 are also determined through batch reactor experiments. For the bidentate surface complexes, the dissolution rate at monolayer ligand surface coverage slows in the order oxalate, glutarate, to malonate. Linear relationships are found between the ligand-promoted dissolution rate constants and both the Langmuir binding constants and the second acidity constants. In contrast, succinate and adipate form monodentate surface structures that dissolve slowly, if at all. In this manner, a connection is established between the macroscopic dissolution rate and the microscopic surface complexation structures. Copyright © 2001 Elsevier Science Ltd

### 1. INTRODUCTION

Organic ligand adsorption to mineral surfaces regulates several environmentally significant chemical reactions, such as dissolution (Furrer and Stumm, 1986), cation sorption (Collins et al., 1999), and photochemistry (Martin et al., 1996). Proton consumption (i.e., an increase in alkalinity) and redox-active Fe(III) release accompany hematite ( $\alpha$ -Fe<sub>2</sub>O<sub>3</sub>) dissolution, as follows:



The rate of the proton-catalyzed dissolution (Eqn. 1) is often slow compared to the rates of ligand-promoted dissolution:



Microbes and roots release carboxylate-rich organic compounds, presumably to facilitate the release of nutrients, including aqueous iron, from the soil matrix (Curl and Truelove, 1986; Jones, 1998). The ligands form inner-sphere complexes with surficial  $>\text{FeOH}$  groups and promote the release of Fe(III) from the oxide lattice (Stone, 1996). The intrinsic dissolution rate depends upon the complexation structure formed between the organic ligand and the surface hydroxyl groups (Furrer and Stumm, 1986; Stumm and Wieland, 1990).

The complexation structures can be classified by infrared surface spectroscopy (Parfitt and Farmer, 1977; Tejedor-Tejedor and Anderson, 1986; Tejedor-Tejedor et al., 1990; Hug and Sulzberger, 1994; Martin et al., 1996; Hug, 1997; Dobson and

McQuillan, 1999). Common structural classifications (Fig. 1) for oxygenated chelating ligands include bidentate mononuclear (C), bidentate binuclear (D), and monodentate mononuclear (E and F) (Hug and Sulzberger, 1994). A bidentate mononuclear complex forms between two oxygen moieties of the ligand and a single electrophilic metal atom on the mineral oxide surface. In a bidentate binuclear structure, the oxygen moieties bridge two metal atoms. A monodentate mononuclear complex forms between a single oxygen moiety and a metal atom; the remaining oxygen atom may be protonated or deprotonated.

In the current study, we employ a homologous series of dicarboxylic acids, including oxalate, malonate, succinate, glutarate, and adipate, to study the effect of chain length on the nature of the surface complexation structures formed on hematite. The surface structures are investigated by infrared spectroscopy. In addition, the ligand-promoted dissolution rates are measured in a batch reactor containing hematite and the same homologous series of ligands. The ligand-promoted dissolution rates of many metal oxides and common aluminosilicates have been determined previously (Huang and Keller, 1971; Cornell et al., 1973; Schnitzer and Kodama, 1976; Furrer and Stumm, 1986; Miller et al., 1986; Zinder et al., 1986; Stone, 1987; Carroll-Webb and Walther, 1988; Wogelius and Walther, 1991; Ludwig et al., 1996). The present study advances the scientific understanding of mineral dissolution by quantitatively relating dissolution rates to spectroscopically determined surface complexation structures.

### 2. EXPERIMENTAL

#### 2.1. Hematite Preparation and Characterization

We employ a standard synthetic method outlined by Schwertmann and Cornell (1991) to prepare a hematite sample of reproducible

\* Author to whom correspondence should be addressed (smartin@deas.harvard.edu).

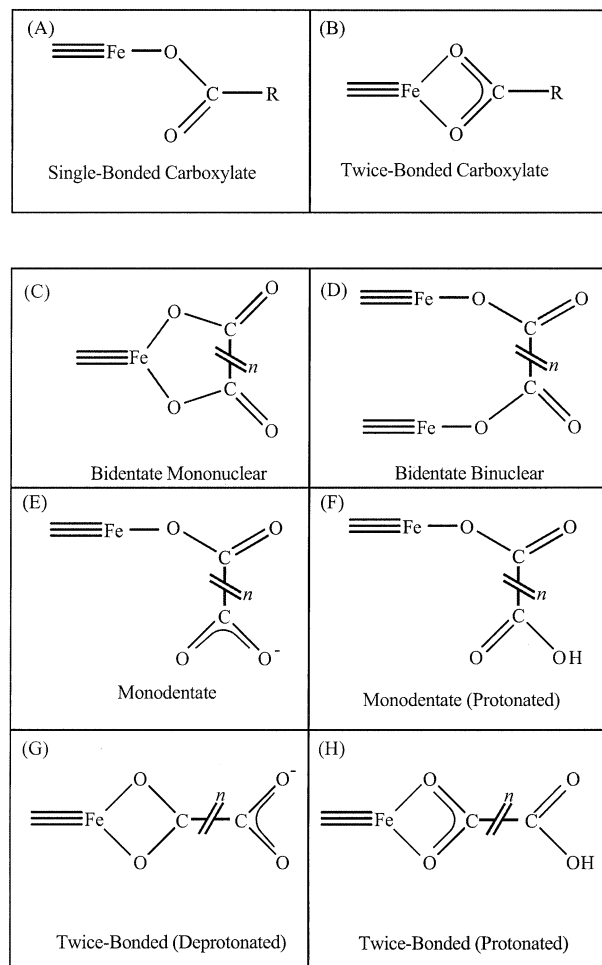


Fig. 1. Proposed surface complexation structures formed between surface hydroxyl groups of iron oxide and a generalized carboxylate moiety (A, B) or a  ${}^{-}\text{OOC}(\text{CH}_2)_n\text{COO}^{-}$  dicarboxylate ligand (C–H).

characteristics. 4.05 g of  $\text{FeCl}_3 \cdot 6\text{H}_2\text{O}$  (Fisher, reagent grade) is dissolved in 750 mL of 1 mM HCl in a 1-L round bottom flask. The translucent yellow solution is refluxed at  $98^\circ\text{C}$  for 7 d and stored in a 1-L stoppered flask in the dark at  $4^\circ\text{C}$  until needed. Just before conducting dissolution experiments, the red, opaque suspension is centrifuged in a 1-L polyethylene bottle for 30 min at 4800 rpm. The supernatant is discarded, and the collected solid residue (typically 1.0 g, percent yield > 85%) is resuspended in 300 mL of deionized water (Nanopure, 18  $\text{M}\Omega$  cm) and sonicated (Fisher Scientific FS30) for 20 min. The suspension is employed in this form for the dissolution experiments. A fresh suspension is synthesized for each dissolution experiment.

Particles are prepared for transmission electron microscope (TEM) imaging by diluting a suspension fourfold with ethanol (Mallinckrodt, Reagent Grade). Next, a single drop of the suspension is placed on a formvar TEM grid (Ted Pella Science, Redding, CA) using a 200- $\mu\text{L}$ -capacity micropipette. The grid is air-dried until no moisture is apparent. The particles are imaged on a Philips CM12 transmission electron microscope operated at 120 KeV (Fig. 2A). Selective area electron diffraction (SAED) patterns are obtained with a JEOL 2000FX transmission electron microscope operated at 200 KeV (Fig. 2B).

Particles are prepared for Brunauer-Emmett-Teller (BET) surface area measurement by drying 1 L of suspension on several watch glasses in a furnace at  $90^\circ\text{C}$  for 6 h. The residue is ground to a fine powder with an alumina mortar and pestle and is subsequently transferred to a precision glass cell and heated at  $120^\circ\text{C}$  under a steady flow of dry

nitrogen for 12 h to further dry the sample. The sample is analyzed by a 3-point BET method on a Quantachrome NOVA 1200 High Speed Gas Sorption Analyzer. Replicate measurements agree within 5%. The drying and grinding, which is necessary to disaggregate particles for BET analysis, may affect grain size and surface area, as compared to the wet suspensions employed in the dissolution experiments. Any differences, however, appear to be small because analysis of the TEM images of the particles deposited from suspension is consistent with the BET surface area determination.

## 2.2. Infrared Measurements

IR spectra of the surface structures formed between the ligands and hematite are collected by attenuated total reflectance (ATR) spectroscopy (Martin et al., 1996). A ZnSe crystal ( $45^\circ$  trapezoid,  $80\text{ mm} \times 10\text{ mm} \times 4\text{ mm}$ ) is employed in a horizontal ATR accessory (Pike Technologies, HATR 022 to 1042, Madison, Wisconsin) placed into the sample compartment of a Nicolet Magna 560 Infrared Spectrophotometer equipped with a DTGS detector. Typically, 1024 scans at a resolution of  $4\text{ cm}^{-1}$  are employed. The background spectrum is the dry ATR element in dry,  $\text{CO}_2$ -free air. Occasionally, smoothing is necessary to eliminate trace gaseous water vapor lines.

In the first step of the procedure, the crystal element (ZnSe) is coated with hematite crystals by applying 2 mL of a 70:30 (v/v) water:ethanol suspension ( $4.9\text{ g L}^{-1}$  hematite) in a thin layer. The addition of ethanol to the mixture enhances evaporation, improves particle adhesion to the crystal, and yields more uniform coatings. The total mass of hematite applied to the surface is 3 mg. After drying at ambient temperature in a desiccator, the surface is washed with a gentle stream of deionized water until no hematite detaches from the surface. With practice, this method is successful in obtaining reproducible red, semiopaque coatings. The coating shows no sign of degradation through the duration of an experiment (2 d maximum). The coating can be removed from the crystal by placing it in a laboratory ultrasonic bath until the surface is restored to a mirror-like luster, typically 1 h.

In the next step, deionized water (Nanopure, 18  $\text{M}\Omega$  cm) is placed onto the ATR element via Luer-lock feed-throughs, and an absorbance spectrum (#1) is recorded. A volume of 20 mL of solution containing aqueous ligand at pH = 5.0 is placed on the ATR element via the feed-throughs (the volume of the sample chamber is under 1 mL; the excess solution flushes the system and flows to waste), and another absorbance spectrum (#2) is recorded after a 30-min equilibration period. Spectra recorded at longer times showed no difference from those collected at 30 min. A new hematite coating is used for each series of ligands.

The aqueous stock solutions are prepared from sodium oxalate (Fisher, 99.5%), malonic acid (Fisher, Reagent Grade), sodium succinate monohydrate (Fisher, Laboratory Grade), glutaric acid (Aldrich, 99%), adipic acid (Fisher, Certified), hydrochloric acid (ACS Plus), and sodium hydroxide (Fisher, Certified). Acetate is not employed as a buffer in these experiments to avoid interferences from its  $\nu(\text{CO}_2)$  bands. However, possible changes in pH arising from adsorption are ruled out by the flushing of the chamber with excess solution. Ionic strength is not set to a fixed value but is estimated as  $I = 0.2$  to 20 mM. Differences in surface adsorption due to electric double layer effects stemming from this variation in ionic strength are assumed to be small (Dzombak and Morel, 1990). No effort is made to remove  $\text{CO}_2$  from solutions; ferric carbonate complexes are not significant in the speciation of ferric iron at low pH values at atmospheric  $p\text{CO}_2$  (Bruno et al., 1992; Bruno and Duro, 2000). Ferric-carbonate complexes are also thus excluded from our analysis of surface adsorbates.

Spectrum #2 contains contributions from the aqueous ligand, the hematite coating, the ligand surface complexation structures, and the solvent water. Subtraction of spectrum #1 reveals contributions from the aqueous ligand and the ligand surface complexation structures. The minimum infrared sensitivity for an aqueous species is  $\sim 1\text{ mM}$  whereas adsorbates yield adequate infrared absorbance at concentrations as low as  $10\text{ }\mu\text{M}$  aqueous concentration: adsorption onto the hematite coating concentrates the aqueous ligand into a spatial region probed by the evanescent wave. Water has a large absorbance near  $1700\text{ cm}^{-1}$ . Strong inner-sphere complexes can shift the asymmetric carboxylate stretch into this spectral region. In these cases, careful measurements (e.g., fresh backgrounds to avoid instrument drift) are

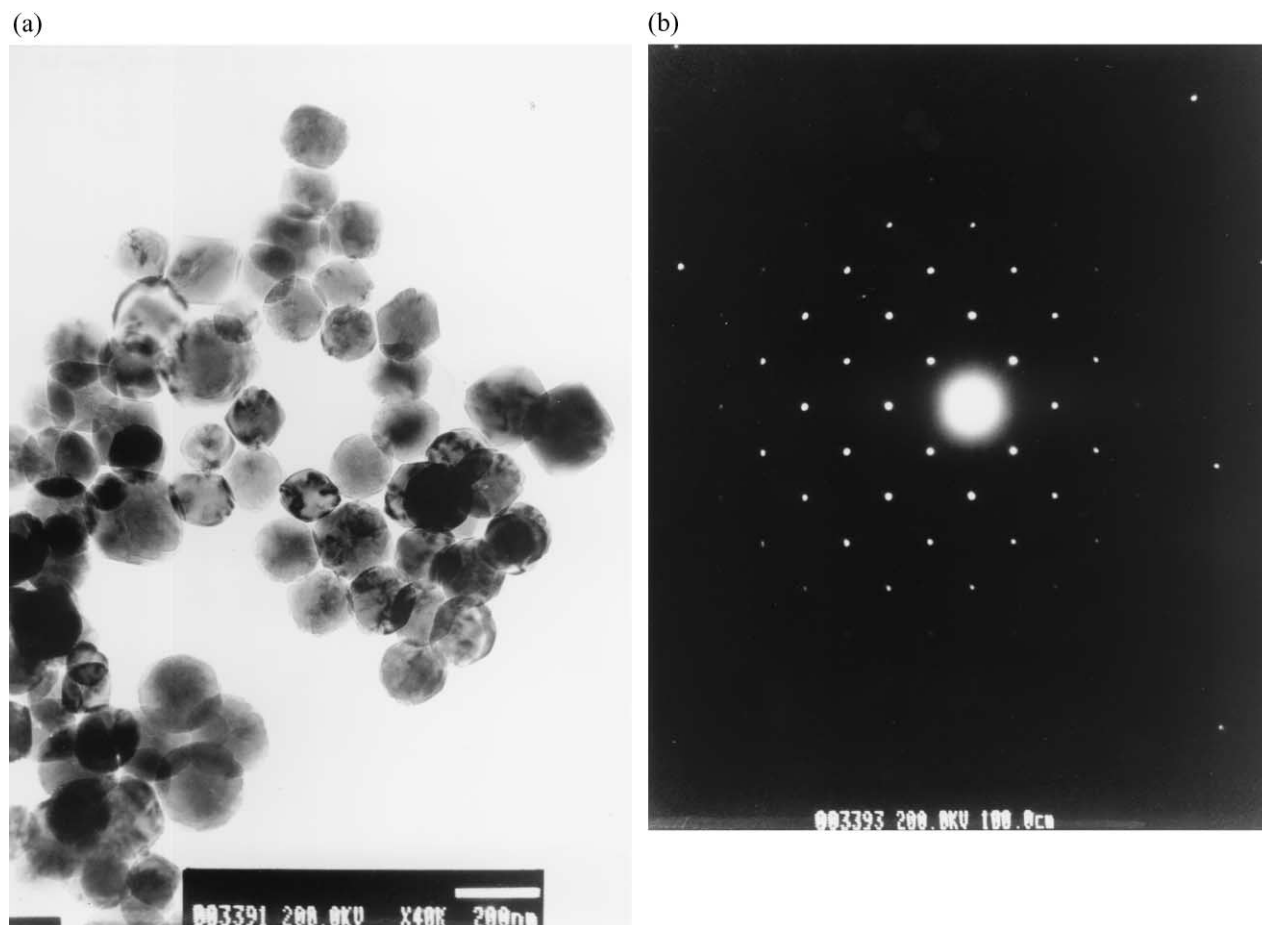


Fig. 2. (A) Transmission electron micrograph and (B) selective area electron diffraction (SAED) pattern of synthetic hematite particles employed in this study. Images provided courtesy of Jia Li and Peter R. Buseck, Arizona State University.

necessary, and the subtraction procedure must be accompanied by manual adjustment of the two spectra for coincident bandlines. Furthermore, replicate experiments are especially important because the subtraction artifacts introduced by instrument drift are random whereas the true signal is consistent.

Spectra of aqueous ligands at pH = 5.0 are recorded in a similar manner. A background spectrum in dry, CO<sub>2</sub>-free air is collected. Deionized water is placed on the uncoated ZnSe ATR element via feed-throughs and an absorbance spectrum is recorded. Aqueous ligand from the stock solutions is then injected onto the element and another spectrum is recorded. The difference between these spectra is the absorbance of the dicarboxylate ligand in the aqueous phase.

### 2.3. Infrared Analysis

Singular value decomposition (SVD) is utilized to analyze the series of IR spectra collected while varying the master variable (viz. the aqueous ligand concentration) (Hug and Sulzberger, 1994; Martin et al., 1996). As the master variable changes, both the concentration and the chemical form of the individual species present may change along with their corresponding contributions to the IR spectra. When the infrared absorbance at a given wavenumber is considered as a channel of data, the variation of the infrared spectra (typically 400 channels) is a strongly covariant data set in highly multidimensional space. However, due to the covariance of absorbance spectra, the highly multidimensional space is in practice spanned by a much smaller subspace. In a single spectrum, covariance arises from absorbance bands. Across several spectra, the Beer-Lambert law contributes to covariance. Multivariate statistical methods, such as SVD (Kleinbaum et al., 1988), can

thus be applied to obtain both a basis of the data set (viz. eigenvectors) and the number of statistically significant independent spectral components. For further explanation of the analysis method, see Martin et al. (1996) and Duckworth (2000).

We employ SVD calculations to determine the number and type of surface complexation structures formed between hematite and the dicarboxylate ligands. The Beer-Lambert law describes the linear response of aqueous absorbance to aqueous ligand concentration. A Langmuir adsorption isotherm is employed to describe the ligand surface concentration as a function of aqueous concentration (Stumm and Morgan, 1996):

$$\theta = \frac{K[A]}{1 + K[A]} \quad (3)$$

where  $\theta$  is the fractional surface coverage from 0 to 1,  $K$  is the Langmuir binding constant between the surface and the ligand, and  $[A]$  is the aqueous ligand concentration. Other candidate adsorption models (e.g., Freundlich or two-site Langmuir models) that we considered are ruled out because they add physical complexity without reduction of the variance of the residuals in the model fit. For bidentate binuclear bonding, the interpretation of  $K$  is an effective binding constant including both chemical and surface geometrical effects (e.g., site blocking and binding site arrangement [Benjamin, 2000]). The SVD calculations are completed in *Mathematica* (Wolfram Research, Inc., Champaign, IL), and the optimization is carried out using the geometric simplex method (Carley and Morgan, 1989).

Previous workers have utilized Fourier transform infrared-attenuated total reflectance (FTIR-ATR) spectroscopy to determine adsorp-

tion behavior of ligands as a function of concentration (Hug and Sulzberger, 1994; Martin et al., 1996; Hug, 1997). Due to the difficulty of determining the total amount of reactive hematite surface area on the ATR element, an absolute surface concentration cannot be calculated. Even so, fractional surface coverages ( $\theta$ ) and Langmuir binding constants ( $K$ ) are determined by the model fit. In a test of the accuracy of  $K$  determined by this method, Martin et al. (1996) found that  $K$  values determined by SVD analysis of IR spectra agree with those obtained by more traditional techniques of adsorption isotherm measurements.

#### 2.4. Dissolution Experiments

Prepared suspensions (section 2.1) are diluted to 400 mL. The pH of this suspension is typically 4. Ligand and sodium acetate (Fisher, ACS certified grade) are subsequently dissolved in the suspension. The pH is adjusted as necessary to 5.0 by the addition of aqueous NaOH or HCl; the acetate (5 mM total acetate/acetic acid concentration) buffers the system. The suspension is diluted with deionized water to the final target volume of 500 mL and placed into the reactor. Ionic strength is estimated to be  $I = 10$  to 30 mM. Typical particulate loadings are 2 g L<sup>-1</sup>.

The reactor is a 1.5-L Pyrex lyophilization bell jar immersed in a constant temperature bath (25°C). The apparatus is periodically inspected; particle adhesion to the walls is not observed. The top piece of the reactor has feed-throughs for an overhead stirrer, a gas sparger, a sampling port, and a pH electrode. Argon (99.997%), passed through a humidifier, continuously sparges the suspension at 200 mL min<sup>-1</sup>, thus excluding atmospheric gases, including O<sub>2</sub> and CO<sub>2</sub>. Aluminum foil, encasing the entire apparatus, excludes light and thus obviates photochemistry.

In a typical dissolution experiment, the reactor is sampled 10 times in 72 h by removing 7-mL aliquots, which are then filtered through 0.2- $\mu$ m mixed cellulose ester membrane syringe filters. Particles in suspension aggregate, causing the scattering of visible light. No particles were observed to pass through the filter, and high iron concentrations associated with filter breakthrough were absent. In this way, the aqueous iron is separated from the suspended particles. The 10 filtrates are stored in the dark at 4°C for up to 1 month. Aqueous iron is quantified by inductively coupled plasma atomic emission spectroscopy (ICP-AES, Perkins-Elmer Plasma 40 Emission Spectrophotometer), which has a sensitivity limit of 0.5  $\mu$ M and an uncertainty of under 10% for the typical 5 to 100  $\mu$ M aqueous iron concentrations of our experiments. Immediately after sampling, select samples are also measured colorimetrically by the phenanthroline method (1  $\mu$ M minimum detection level) to verify the absence of Fe(II) (Greenberg et al., 1992).

### 3. RESULTS

The synthesized particles are characterized for their crystallinity, size, and surface area. TEM micrographs show polyhedral particles on the order of 200 nm in diameter (Fig. 2A). The BET specific surface area of the particles is 1.7 m<sup>2</sup> g<sup>-1</sup>, corresponding to a monodisperse spherical particle diameter of 670 nm. The particles are well-crystallized hematite based on analysis of  $d$ -spacings obtained from SAED (Fig. 2B).

Figure 3 shows aqueous IR spectra measured at pH = 5.0 for five carboxylate ligands (60 mM concentration). The peak positions between 1250 and 2000 cm<sup>-1</sup> in the spectra for the aqueous ligands measured in this study at pH = 5.0 are shown in Table 1 along with literature comparisons. Also given are the peak positions of the spectra of the aqueous components derived from SVD. The peak positions agree within 5 cm<sup>-1</sup>, which is comparable to the spectral resolution of 4 cm<sup>-1</sup>, with the aqueous spectra derived from this study and those available in the literature (Cabaniss et al., 1998; Dobson and McQuillan, 1999). For all carboxylate stretches, the peak positions of SVD linear components are within 5 cm<sup>-1</sup> of the aqueous peak

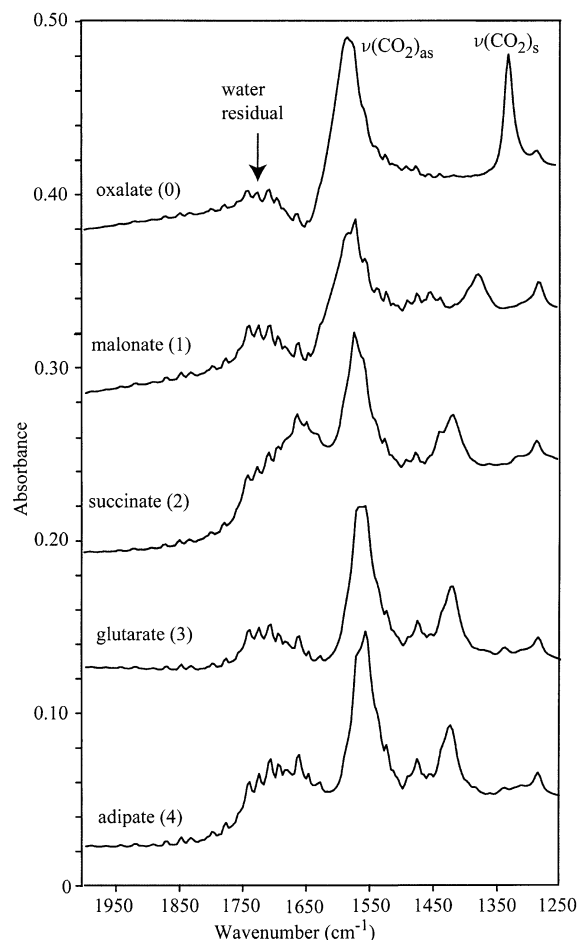


Fig. 3. ATR infrared spectra of 60 mM aqueous oxalate, malonate, succinate, glutarate, and adipate recorded at pH = 5.0.

maxima both measured by us and cited in the literature (Table 1).

Figure 4 shows IR-ATR spectra of aqueous oxalate and oxalate bound to hematite at 0.06, 0.12, 0.3, 0.6, 1.2, 3.0, and 6.0 mM total oxalate concentration and pH = 5.0, along with the residuals after modeling. The surface coverage model fit yields a Langmuir binding constant,  $K$ , of 30,000 mM/L<sup>-1</sup>. The columns on the right-hand side indicate the relative contribution of the linear and Langmuir components to the spectra. Both columns are scaled independently from 0 to 1. The linear component is scaled as a fraction of the maximum concentration, and the Langmuir component is scaled as fractional surface coverage,  $\theta$ . In all cases,  $\theta$  approaches unity at ligand concentration of 6 mM, indicating monolayer coverage. The model does not account for the depletion of aqueous ligand by surface adsorption, which is equivalent to the assumption that the available surface of the coating does not adsorb enough ligand to appreciably change the aqueous ligand concentration. There is some structure in the residuals of the 0.06 and 3.0 mM spectra, indicating a slight underprediction of adsorption by the model, possibly arising from the surface electric field effects (i.e., generalized electric double layer) not included in the Langmuir model (Dzombak and Morel, 1990). The residuals strongly covary with the basis spectra themselves (e.g., com-

Table 1. Infrared peak positions ( $\text{cm}^{-1}$ ) of linear spectral components (SVD analysis), measured aqueous carboxylate spectra (this work), and literature spectra.

Ligand	Linear component	Aqueous species	Dobson and McQuillan, 1999	Cabaniss et al., 1998	Assignment
Oxalate	1571	1568	1570	1569	$\nu_{\text{as}}(\text{CO}_2)$
	1312	1306	1307	1307	$\nu_{\text{s}}(\text{CO}_2)$
Malonate	1562	1565	1564	1561	$\nu_{\text{as}}(\text{CO}_2)$
	1355	1358	1355	1356	$\nu_{\text{s}}(\text{CO}_2)$
Succinate	1554	1549	1550	1552	$\nu_{\text{as}}(\text{CO}_2)$
	1404	1400	1393	1395	$\nu_{\text{s}}(\text{CO}_2)$
Glutarate	1547	1550	N/A	1547	$\nu_{\text{as}}(\text{CO}_2)$
	1402	1399	N/A	1401	$\nu_{\text{s}}(\text{CO}_2)$
Adipate	1552	1547	1546	N/A	$\nu_{\text{as}}(\text{CO}_2)$
	1413	1403	1403	N/A	$\nu_{\text{s}}(\text{CO}_2)$

pare Fig. 9 with the residual in Fig. 4), which supports the application of a one-site adsorption model while also indicating that a quantitative formulation with a single parameter (viz.  $K$  in the Langmuir model) is an oversimplification. A one-site model with two or more parameters would possibly improve

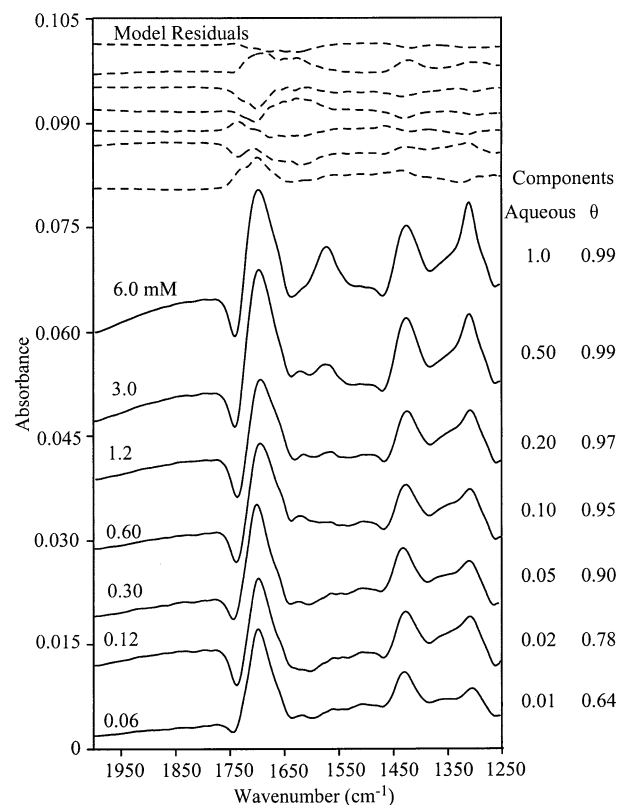


Fig. 4. ATR infrared spectra of 0.06, 0.12, 0.30, 0.60, 1.2, 3.0, and 6.0 mM aqueous oxalate recorded with a hematite-coated ATR element. The residuals of a model fit are shown (top). In the model, orthogonal components obtained from singular value decomposition are obliquely rotated to generate physical IR spectra. One factor contributes linearly and the other in a Langmuir fashion to the recorded spectra. On the right side of the figure, contributions of the linear aqueous component (arbitrarily scaled) and the Langmuir component, shown as fractional surface monolayer coverage, are given. Spectra are offset for clarity. Conditions: pH = 5.0,  $\alpha\text{-Fe}_2\text{O}_3$  loading = 3 mg, and 25°C.

the fit. For our purposes, it is sufficient to indicate that the residuals for oxalate, malonate, glutarate, and succinate are consistent with a single surface structure.

Similar results are shown in Figures 5–8 for malonate, glutarate, succinate, and adipate, respectively. The Langmuir binding constants are summarized in Table 2. The variation from one figure to the next in the absolute magnitude of the absorbance values arises from changes in the thickness of the iron oxide coating from one set of measurements to the next. The variation does not affect the qualitative form of the spectra or our interpretation. In Figure 8 (adipate), the model performs poorly, as indicated by the larger residuals (Table 2).

The variance of the concentration-dependent spectral series

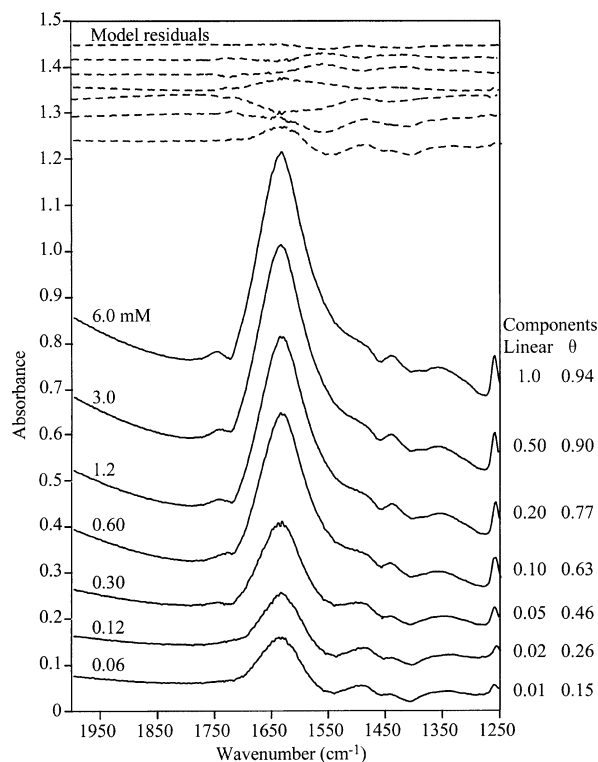


Fig. 5. ATR infrared spectra of 0.06, 0.12, 0.30, 0.60, 1.2, 3.0, and 6.0 mM aqueous malonate recorded with a hematite-coated ATR element. The model residuals are shown (top). Conditions: pH = 5.0,  $\alpha\text{-Fe}_2\text{O}_3$  loading = 3 mg, and 25°C.

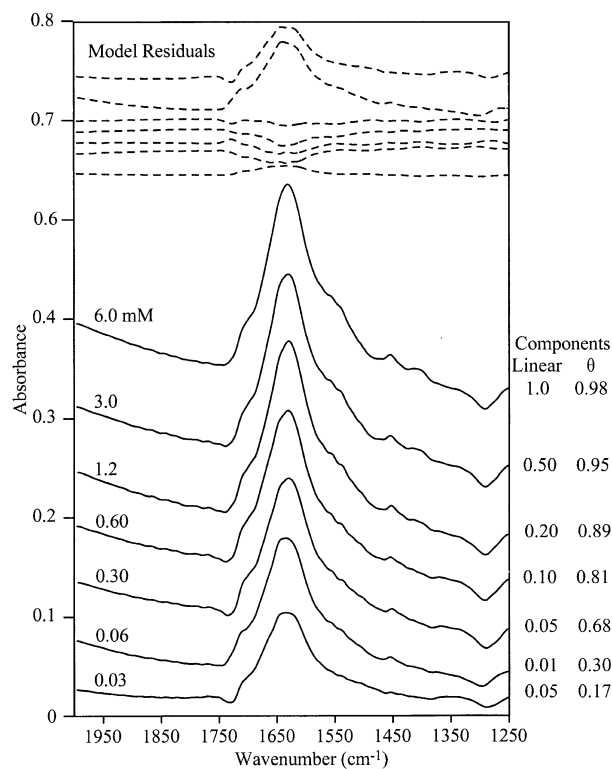


Fig. 6. ATR Infrared spectra of 0.03, 0.06, 0.30, 0.60, 1.2, 3.0, and 6.0 mM aqueous glutarate recorded with a hematite-coated ATR element. The model residuals are shown (top). Conditions: pH = 5.0,  $\alpha$ -Fe<sub>2</sub>O<sub>3</sub> loading = 3 mg, and 25°C.

for each ligand is adequately accounted for by one aqueous species and one surface structure. Figure 9 shows the Langmuir spectral components (i.e., the spectra of the surface complexation structures) of oxalate, malonate, succinate, glutarate, and adipate. Peaks are shifted from those of the aqueous ligands (gray bars), indicating the formation of complexes with the surface iron. Spectra are scaled from zero to unity in arbitrary units because absolute concentration ( $\text{mol m}^{-2}$ ) requires knowledge of coating thickness and morphology, evanescent wave amplitude, and optical constants. Of particular importance is the similarity of the malonate and glutarate spectra and their singular difference from the succinate spectrum, which is a shoulder at  $1547 \text{ cm}^{-1}$ . In replicate measurements and analysis, this difference is consistent and, as discussed below, critical to the assignment of surface structures. The spectroscopic data on surface structures aid in the interpretation of dissolution data.

The release of aqueous iron vs. time is shown in Figure 10 in the presence of 10 mM oxalate, malonate, succinate, glutarate, and adipate at pH = 5.0. The dissolution rates decrease monotonically from oxalate, to glutarate, to malonate. Succinate and adipate do not significantly promote dissolution. The rates do not correlate with carbon chain length:  $n = 0 > 3 > 1 \gg 2, 4$  in  $\text{HOOC}(\text{CH}_2)_n\text{COOH}$ . The rates do not vary within experimental error in replicates conducted for each ligand. At all times, the system is far from equilibrium because the concentration of the ligand is much greater than that of dissolved iron, causing the iron in solution to be dominantly in the form of

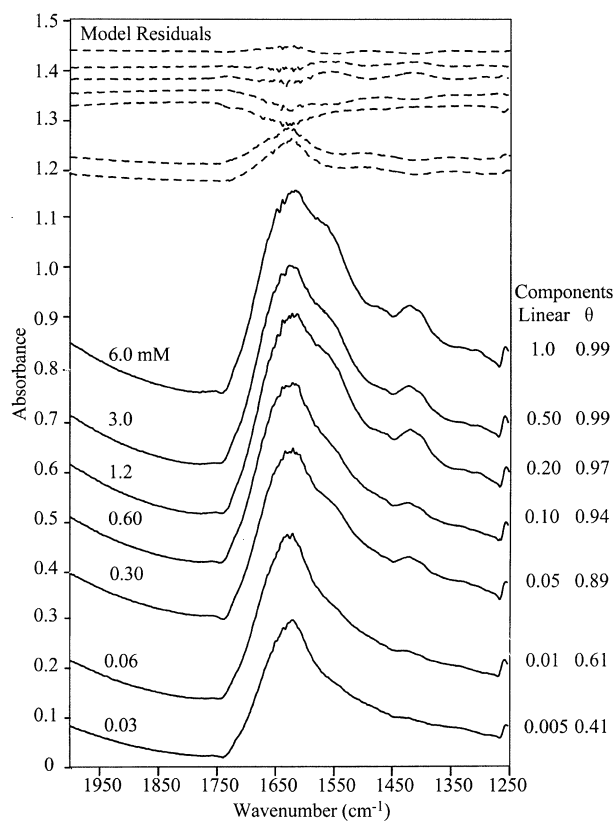


Fig. 7. ATR Infrared spectra of 0.03, 0.06, 0.30, 0.60, 1.2, 3.0, and 6.0 mM aqueous succinate recorded with a hematite-coated ATR element. The model residuals are shown (top). Conditions: pH = 5.0,  $\alpha$ -Fe<sub>2</sub>O<sub>3</sub> loading = 3 mg, and 25°C.

organic complexes, greatly increasing the aqueous solubility of iron. The formation constant of acetate with ferric iron is several orders of magnitude lower than those of the dicarboxylate ligands (Martell and Smith, 1977), and thus acetate should negligibly influence both surface complexation and aqueous iron speciation. During dissolution (10 mM ligand), the ligand surface coverage is unity as determined from the IR adsorption isotherm measurements, notwithstanding speciation differences among the aqueous ligands. Colorimetric tests detected no Fe(II) in any sample, indicating that the dissolution process is not reductive.

## 4. DISCUSSION

### 4.1. Aqueous Species

The linearly contributing spectral components are assigned as aqueous dianions based upon the close agreement between observed peak positions and reference values (Table 1) at pH = 5.0. Based on the acidity constants for these ligands, protonated species are expected in the aqueous phase. Published spectra (Cabaniss et al., 1998) for these aqueous ligands indicate that, for the dicarboxylate species other than oxalate, only a small change occurs in the peak position of the asymmetric and symmetric stretches with a change in speciation from  $^-\text{OOC}(\text{CH}_2)_n\text{COO}^-$  to  $\text{HOOC}(\text{CH}_2)_n\text{COO}^-$ . The  $\nu(\text{C}=\text{O})$  and  $\nu(\text{C}-\text{OH})$  of dicarboxylate bands have low absorption intensi-

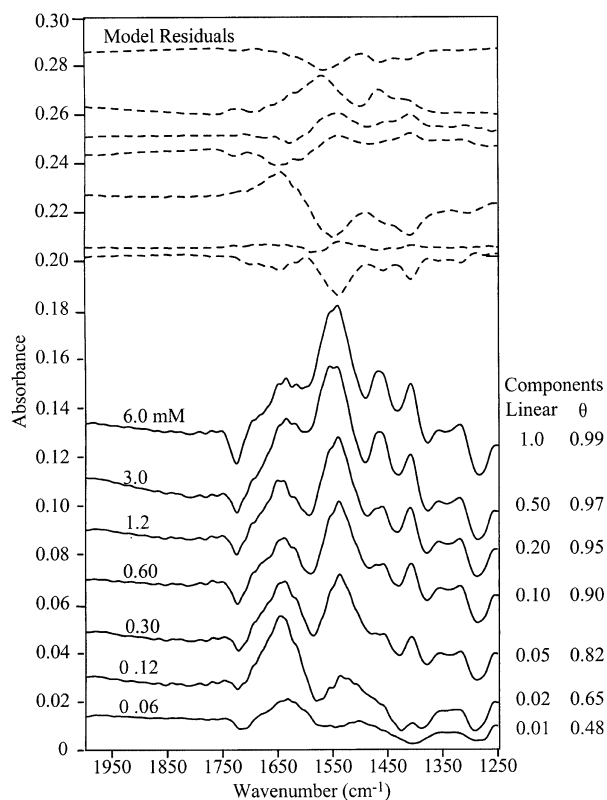


Fig. 8. Infrared spectra of 0.06, 0.12, 0.30, 0.60, 1.2, 3.0, and 6.0 mM aqueous adipate recorded with a hematite-coated ATR element. The model residuals are shown (top). Conditions: pH = 5.0,  $\alpha$ -Fe<sub>2</sub>O<sub>3</sub> loading = 3 mg, and 25°C.

ties as compared to  $\nu(\text{CO}_2)$  bands at pH = 5.0 (Cabaniss et al., 1998). The IR spectral signature of the  $\text{HOOC}(\text{CH}_2)_n\text{COO}^-$  species is effectively absent at this pH.

#### 4.2. Surface Structures

The Langmuir components of the IR spectra of the dicarboxylate ligands contain peaks shifted 50 to 130  $\text{cm}^{-1}$  from their aqueous counterparts. As such, the surface structure corresponding to the Langmuir component is an inner-sphere

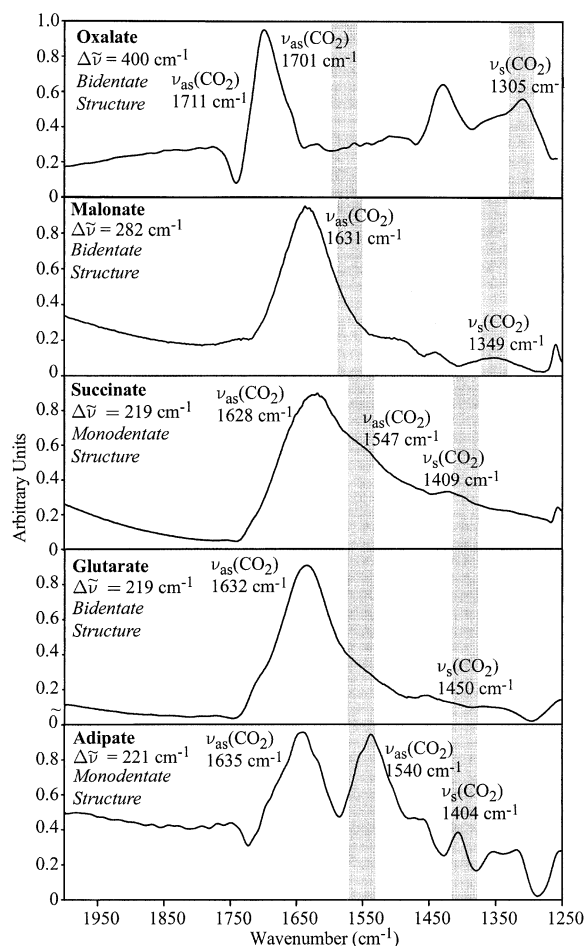


Fig. 9. Infrared spectra of the surface-adsorbed complexes of oxalate, malonate, succinate, glutarate, and adipate on hematite, as obtained by oblique rotation of SVD orthogonal components constrained to a Langmuir adsorption model. Peak positions for carboxylate stretches are shown.  $\Delta\bar{\nu}$  is the difference between  $\nu_{\text{as}}(\text{CO}_2)$  and  $\nu_{\text{s}}(\text{CO}_2)$ . For comparison, gray bars indicate the absorption regions of  $\nu_{\text{as}}(\text{CO}_2)$  and  $\nu_{\text{s}}(\text{CO}_2)$  vibrations of the aqueous species, as provided in Table 1.

complex (Hug, 1997). In comparison, outer-sphere complexes exhibit little shift in the  $\nu(\text{CO}_2)$  bands (Nordin et al., 1997). Our results are consistent with the work of Filius et al. (1997)

Table 2. Physical data and experimental results.<sup>a</sup>

Ligand	Formula	pK <sub>a1</sub>	pK <sub>a2</sub>	pH	Rate (mol m <sup>-2</sup> s <sup>-1</sup> )	Rate constant, <i>k</i> (s <sup>-1</sup> )	Langmuir binding constant, <i>K</i> (M <sup>-1</sup> )	$\frac{\sum V_{\text{residuals}}}{\sum V_{\text{spectra}}} \times 10^{-2}$
Oxalate (0)	<sup>-</sup> O <sub>2</sub> C <sub>2</sub> O <sub>4</sub> <sup>-</sup>	1.25	4.27	5.0	$1.0 \times 10^{-10}$	$1.5 \times 10^{-5}$	$30000 \pm 3000$	3.7
Malonate (1)	<sup>-</sup> OOC(CH <sub>2</sub> ) <sub>1</sub> COO <sup>-</sup>	2.85	5.70	5.0	$1.4 \times 10^{-11}$	$2.0 \times 10^{-6}$	$3000 \pm 300$	1.3
Succinate (2)	<sup>-</sup> OOC(CH <sub>2</sub> ) <sub>2</sub> COO <sup>-</sup>	4.42	5.42	5.0	$<2.8 \times 10^{-12}$	$<4.1 \times 10^{-7}$	$2700 \pm 300$	4.7
Glutarate (3)	<sup>-</sup> OOC(CH <sub>2</sub> ) <sub>3</sub> COO <sup>-</sup>	4.34	5.43	5.0	$3.3 \times 10^{-11}$	$4.8 \times 10^{-6}$	$7200 \pm 700$	1.1
Adipate (4)	<sup>-</sup> OOC(CH <sub>2</sub> ) <sub>4</sub> COO <sup>-</sup>	4.21	5.64	5.0	$<2.8 \times 10^{-12}$	$<4.1 \times 10^{-7}$	N/A	11

<sup>a</sup> The numbers in parentheses give the carbon chain length, *n*, in <sup>-</sup>OOC(CH<sub>2</sub>)<sub>*n*</sub>COO<sup>-</sup>. The pK<sub>a</sub> values are from Martell and Smith (1977). Rates of aqueous iron release (mol m<sup>-2</sup> s<sup>-1</sup>) in hematite suspensions containing various dicarboxylate ligands and the associated kinetic rate constants (s<sup>-1</sup>) are shown. Also given are the Langmuir binding constants, *K* (M<sup>-1</sup>), determined by the SVD analysis and the ratio of the variance of the residuals of the model fit to the variance of the infrared data for oxalate, malonate, succinate, glutarate, and adipate. Conditions: 5 mM acetate buffer, pH = 5.0, 2 g L<sup>-1</sup> hematite, 25°C.

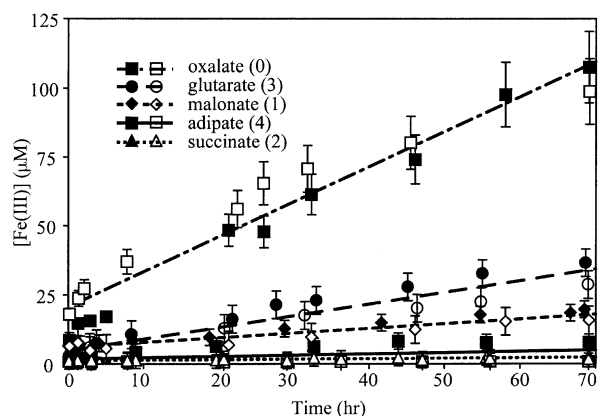


Fig. 10. Dissolution studies. Aqueous iron concentration vs. time in the presence of oxalate, glutarate, malonate, adipate, and succinate. Release rates in the presence of adipate and succinate are not distinguishable from control measurements. The number in parentheses is  $n$  in  $^-\text{OOC}(\text{CH}_2)_n\text{COO}^-$ . Lines are to aid the eye and do not indicate a model fit. Open and closed markers show replicate trials. Conditions: 5 mM acetate buffer, pH = 5.0, 2 g L $^{-1}$  hematite, 25°C.

who report inner-sphere complexation for di- and tricarboxylate ligands on goethite. Surface complexation structures that we postulate to exist between dicarboxylate ligands of the  $^-\text{OOC}(\text{CH}_2)_n\text{COO}^-$  series and hematite surface groups are depicted and labeled in Figure 1. Single moieties can interact with the surface from one (single-bonded, e.g., A) or two (twice-bonded, e.g., B) oxygen atoms. Structures can also be classified based on the number of moieties interacting with the surface. Monodentate structures bind through one carboxyl group (e.g., E and F) whereas bidentate structures interact through two moieties (chelating, e.g., C and D). Those complexes bridging two surface iron atoms are binuclear (e.g., D).

### 4.3. Assignment of Surface Structures

We employ two tools to assign the infrared Langmuir spectral components (Fig. 9) as surface complexation structures depicted in Figure 1. First, we make direct comparisons between these spectra and those in the literature for bidentate transition metal salts (Fujita et al., 1962; Dobson and McQuillan, 1999). In this way, we differentiate between one or both carboxylate moieties interacting with surficial iron. Second, we recognize that one or both of the oxygen atoms of a single

carboxylate moiety can interact with a surficial iron atom. Single- and twice-bonded carboxylate moieties are distinguished from one another by a second spectroscopic tool that examines the separation,  $\Delta\tilde{\nu}$ , between  $\nu_{\text{as}}(\text{CO}_2)$  and  $\nu_{\text{s}}(\text{CO}_2)$  of aqueous and surface carboxylate complexes (Deacon and Phillips, 1980; Nara et al., 1996; Dobson and McQuillan, 1999). For free aqueous dicarboxylate species,  $\Delta\tilde{\nu}$  ranges from 150 to 265  $\text{cm}^{-1}$ . Upon binding with a metal atom,  $\Delta\tilde{\nu}$  increases because the symmetry of the group is reduced, broadening the difference between the strength of carbon–oxygen oscillators. Values of  $\Delta\tilde{\nu} > 200 \text{ cm}^{-1}$  indicate a single bond between the metal and the carboxylate group, whereas  $\Delta\tilde{\nu} < 150 \text{ cm}^{-1}$  indicates a twice-bonded structure. In the latter case, the oxygen atoms in the carboxylate functional group may bond to either one (i.e., chelating structure) or two (i.e., bridging structure) metal atoms. Because each group is a bidentate structure bound to an equivalent atom, the difference in energy between the carbon–oxygen oscillators is reduced, and thus the separation between the  $\nu_{\text{as}}(\text{CO}_2)$  and  $\nu_{\text{s}}(\text{CO}_2)$  is reduced.

#### 4.3.1. Bidentate surface complexation structures

The infrared spectrum of the Langmuir component of oxalate determined by the constrained model fit (Fig. 9) is similar to literature spectra of oxalato–metal oxide surface complexes (Table 3). The peak and the shoulder for the  $\nu_{\text{as}}(\text{CO}_2)$  stretch at 1700  $\text{cm}^{-1}$  arise from vibrational coupling between adjacent C=O bonds. Additional peaks of oxalato–metal and oxalato–surface complexes are assigned in Table 3. We assign the spectrum as a bidentate surface structure (Fig. 1C or D) by analogy to the solid bidentate complex  $\text{Na}_2[\text{TiO}(\text{C}_2\text{O}_4)_2]_2$  (Dobson and McQuillan, 1999). This spectral component is consistent with the spectra of oxalate chelating to the surface of several different metal oxides (Rodenas et al., 1997; Dobson and McQuillan, 1999). However, differentiating between bidentate mononuclear (C) and bidentate binuclear structures (D) is not possible from our analysis of infrared data (q.v. section 4.5).

For malonate, the infrared spectrum of the Langmuir component has peaks at 1260, 1349, 1439, and 1631  $\text{cm}^{-1}$ . The peak at 1349  $\text{cm}^{-1}$  is nearly unshifted from  $\nu_{\text{s}}(\text{CO}_2)$ . Based on literature assignments, we attribute the peaks at 1260  $\text{cm}^{-1}$  and 1439  $\text{cm}^{-1}$  to the  $\delta(-\text{CH}_2-)$  bend (Dobson and McQuillan, 1999). The peak at 1631  $\text{cm}^{-1}$  arises from  $\nu_{\text{as}}(\text{CO}_2)$ . Corresponding literature values on titania and alumina are 1593 and

Table 3. Peak positions ( $\text{cm}^{-1}$ ) in the infrared spectra of oxalato–surface and oxalato–metal complexes.

Aqueous oxalate <sup>a</sup>	Adsorbed oxalate					Oxalate salts			Assignment
	Fe <sub>2</sub> O <sub>3</sub> <sup>b</sup>	TiO <sub>2</sub> <sup>c</sup>	ZrO <sub>2</sub> <sup>c</sup>	Al <sub>2</sub> O <sub>3</sub> <sup>c</sup>	Ta <sub>2</sub> O <sub>5</sub> <sup>c</sup>	Na <sub>2</sub> [TiO(C <sub>2</sub> O <sub>4</sub> ) <sub>2</sub> ] <sub>2</sub> <sup>c</sup>	K <sub>3</sub> [Fe(C <sub>2</sub> O <sub>4</sub> ) <sub>3</sub> ] · 3H <sub>2</sub> O <sup>d</sup>		
1568	1720	1711	1708	1720	1711	1713	1712	$\nu_{\text{as}}(\text{CO}_2)$	
	1701	1686	1673	1695	1688	1681, 1630	1675, 1642	$\nu_{\text{as}}(\text{CO}_2)$	
1306	1423	1424	1432	1424	1406		1387	$\nu(\text{C}-\text{O}) + \nu(\text{C}-\text{C})$	
	1305	1271	1284	1297	1266	1256	1253	$\nu_{\text{s}}(\text{CO}_2)$	

<sup>a</sup> This study, 60 mM oxalate at pH = 5.0.

<sup>b</sup> This study, Langmuir model component.

<sup>c</sup> Dobson and McQuillan, 1999.

<sup>d</sup> Fujita et al., 1962.

1597  $\text{cm}^{-1}$ , respectively (Dobson and McQuillan, 1999), while the range of  $\nu_{\text{as}}(\text{CO}_2)$  in literature for iron-carboxylate complexes is 1600 to 1710  $\text{cm}^{-1}$  (Bargar et al., 1999). Because there are only two peaks in the region of the carboxylate modes, each carboxylate functional group interacts in the same manner with the surface. The conclusion is that the complex must form a symmetrical bidentate surface form. For malonate,  $\Delta\bar{\nu} = 282 \text{ cm}^{-1}$ , indicating that the carboxylate group forms a single-bonded surface complex. These facts taken together indicate that malonate forms a bidentate surface structure (i.e., 1C or D) on hematite at  $\text{pH} = 5.0$ .

Glutarate's infrared spectrum of the Langmuir component exhibits peaks at 1250, 1367, 1450, and 1632  $\text{cm}^{-1}$ . The spectrum is similar to malonate and is assigned accordingly. We believe glutarate forms a bidentate surface complexation structure, as depicted in Figure 1C or D, on hematite at  $\text{pH} = 5.0$ .

#### 4.3.2. Monodentate surface complexation structures

The infrared spectrum of the Langmuir component of succinate exhibits peaks at 1255, 1409, 1547, and 1628  $\text{cm}^{-1}$ . The bands at 1409 and 1547  $\text{cm}^{-1}$  have similar locations to the symmetric (1404  $\text{cm}^{-1}$ ) and the asymmetric (1555  $\text{cm}^{-1}$ ) stretches of the aqueous  $\text{R-COO}^-$  anion: we conclude that one carboxylate moiety is not bound to the surface. For the other carboxylate group, we follow a similar rationale as for malonate and attribute the peak at 1628  $\text{cm}^{-1}$  to a shifted  $\nu_{\text{as}}(\text{CO}_2)$ , indicative of a surface-bound group. The corresponding  $\nu_{\text{s}}(\text{CO}_2)$  is not evident, perhaps obscured by overlap with the peak at 1409  $\text{cm}^{-1}$  since little shift occurs for this band in the other structures studied. We then obtain  $\Delta\bar{\nu} = 219 \text{ cm}^{-1}$ , indicating a lone oxygen bound to the surface from this carboxylate group. The corresponding surface complexation structure is depicted in Figure 1E.

For adipate, the infrared spectrum of the Langmuir component exhibits peaks at 1265, 1317, 1358, 1404, 1540, and 1635  $\text{cm}^{-1}$ . Interpretation of the peaks above 1400  $\text{cm}^{-1}$  is analogous to those of succinate. The peaks at 1404 and 1540  $\text{cm}^{-1}$  are unshifted from  $\nu_{\text{as}}(\text{CO}_2)$  and  $\nu_{\text{s}}(\text{CO}_2)$  of aqueous adipate, which we interpret as indicating that one adipate moiety is not bound to the surface. The peak at 1635  $\text{cm}^{-1}$  is assigned as surface-bound  $\nu_{\text{as}}(\text{CO}_2)$  of the other adipate carboxylate moiety. The corresponding  $\nu_{\text{s}}(\text{CO}_2)$  is not apparent, likely overlapping with the peak at 1404  $\text{cm}^{-1}$ . We then obtain  $\Delta\bar{\nu} = 221 \text{ cm}^{-1}$ . This separation indicates a single-bonded carboxylate group. Using the same arguments as for succinate, we assign adipate a monodentate surface structure depicted in Figure 1E. We have no assignment for the three peaks below 1400  $\text{cm}^{-1}$ , which are similarly observed and unassigned at 1265, 1318, and 1362  $\text{cm}^{-1}$  by Dobson and McQuillan (1999) for adipate bound to  $\text{Ta}_2\text{O}_5$ . In contrast to the other ligands, the single-component Langmuir fit is poor for adipate, as shown by the large residuals in Figure 8. For this reason, no Langmuir binding constant is reported in Table 2.

#### 4.4. Relationships between Carbon Chain Length and Surface Structure

A linear trend does not exist between the carbon chain length of  $^- \text{OOC}(\text{CH}_2)_n \text{COO}^-$  ligands and the surface structures

formed at  $\text{pH} = 5.0$ . For example,  $n = 0, 1, 3$  species (viz. oxalate, malonate, and glutarate) form bidentate ring structures whereas the  $n = 2, 4$  species (viz. succinate and glutarate) form monodentate structures. The surface adsorption chemical reactions are shown in Figure 11. The formation of bidentate structures by the short chain ligands ( $n = 0$  and 1) is easily rationalized by analogy to stable 5- and 6-membered heteromolecular organic rings. By this line of reasoning, bidentate surface structure formation by the longer ligands would be accompanied by Pitzer or transannular strain (March, 1992). Monodentate formation would then be more favorable, which in fact is the adopted surface complexation structure for succinate and adipate. Glutarate, however, forms a bidentate structure. To explain this behavior, we note cycloalkanes do not exhibit a monotonic trend of enthalpy of formation per carbon atom. The carbon-normalized ring energies,  $\Delta H_f^\circ/\text{C}$ , vary as follows:  $-15.27, -20.71, -16.94, -15.69$ , and  $-16.52 \text{ kJ/mol}$  for 5- to 9-membered carbon rings, respectively. This variation in the enthalpies of formation is attributed to ring puckering required to preserve bond angles as closely as possible to the unstrained  $sp^3$  angles (Loundon, 1988). The rings formed by dicarboxylate ligands on the oxide surface are heterocyclic, so analogy with cycloalkanes should only give qualitative guidance. Even so, this energy minimization by distortion of the ring structure is also applicable to surface complexation structures. Compared to succinate and adipate, glutarate is apparently able to adopt a bidentate ring structure in an energy-minimized geometry.

The Langmuir binding constants for the dicarboxylate ligands that form bidentate surface complexation structures follow a linear free energy relationship with the second acidity constant for the aqueous species, as shown in Figure 12A. The correlation is as follows:

$$K = -2.0 \times 10^4 \text{ p}K_{\text{a}2} + 1.2 \times 10^5 \quad (4)$$

The correlation is rationalized because the second acidity constant expresses the proclivity of the second carboxylate functional group to accept electron density (i.e., by dissociation) when its counterpart is already deprotonated. The electronic structure of the aqueous dianion form of the ligand is expected to be similar to the adsorbed bidentate ligand because the bonding between iron oxides and adsorbates is dominantly ionic (Anderman and Kennedy, 1988). In this case, the second acidity constant is indicative of the relative ability of a carboxylate to form an ionic association with a surficial iron atom when it is already bound to a metal center. Thus, as  $\text{p}K_{\text{a}2}$  decreases, the affinity of the second moiety for the surface, and thus the overall stability of the complex, increases linearly.

#### 4.5. Ligand-Promoted Dissolution

The change in aqueous iron concentration as a function of time,  $dC/dt$ , is related to the macroscopic dissolution rate,  $R$  ( $\text{mol m}^{-2} \text{ s}^{-1}$ ), by:

$$\frac{dC}{dt} = LS_A R \quad (5)$$

where  $L$  ( $\text{g L}^{-1}$ ) is the loading of the hematite suspension,  $S_A$  is the reactive specific surface area ( $\text{m}^2 \text{ g}^{-1}$ ) approximated by

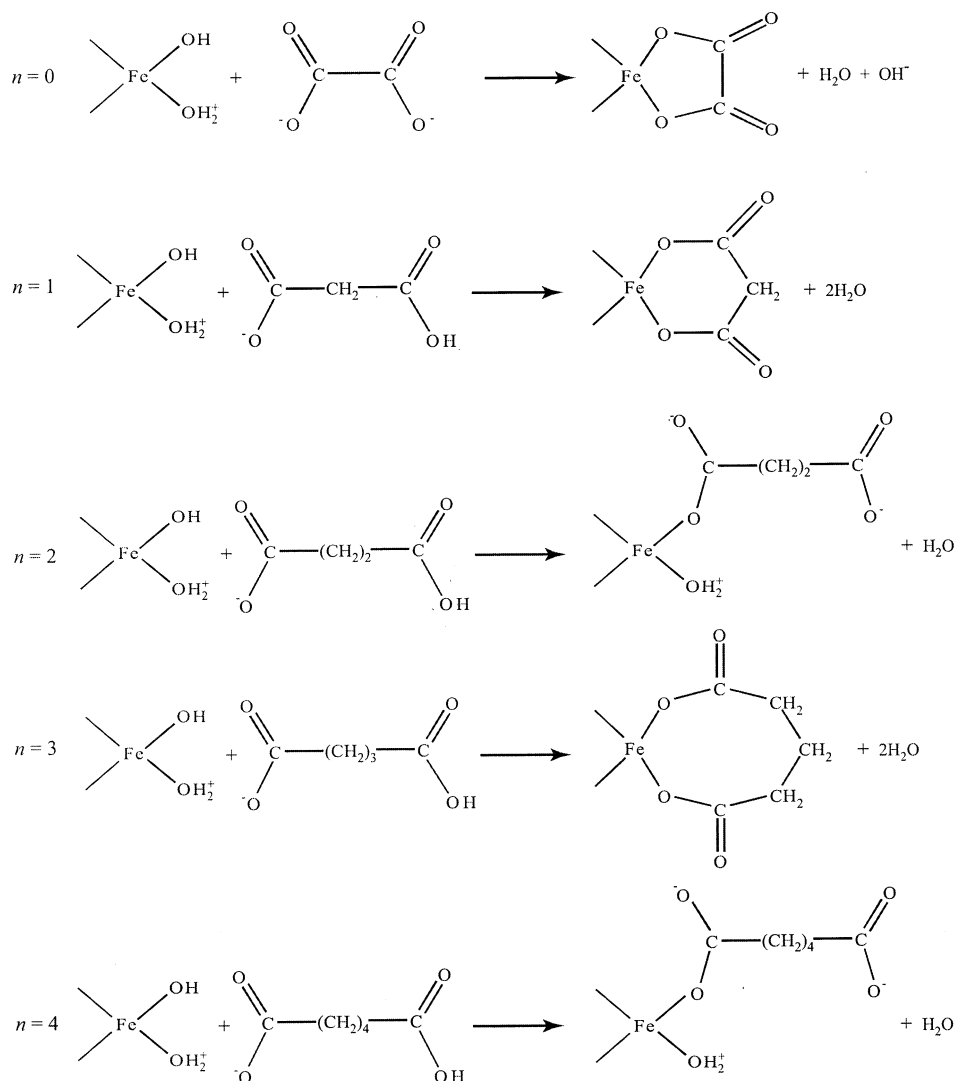


Fig. 11. The proposed surface chemical reactions between oxalate, malonate, succinate, glutarate, and adipate and hematite surface hydroxyl groups at pH = 5.0.

the BET measurements, and  $t$  is time (s).  $L$  and  $S_A$  are assumed to be time-independent. The dissolution results (Fig. 10) show a linear increase in aqueous iron with time. From Eqn. 5, we then infer that the macroscopic dissolution rates are time-independent ( $dR/dt = 0$ ) and proportional ( $1/LS_A$ ) to the slopes of the best-fit lines in Figure 10. The obtained rates for each ligand under various reactor conditions are summarized in Table 2. The reported rate for oxalate-promoted dissolution is within the range ( $8.8 \times 10^{-13}$  to  $1.8 \times 10^{-10}$  mol m<sup>-2</sup> s<sup>-1</sup>) reported in the literature (Zhang et al., 1985; Miller et al., 1986; Zinder et al., 1986; Banwart et al., 1989; Hersman et al., 1995; Maurice et al., 1995). The variation in the literature rates is at least partially attributable to changes in conditions, such as pH (3 to 5) or aqueous oxalate concentration ( $5 \times 10^{-5}$  to 0.1 mol/L), as well as to differing hematite surface pretreatments (e.g., HNO<sub>3</sub> or HF treatment) and particle morphologies (indicative of different dominant crystal faces with different reactivities and thus different macroscopic dissolution rates).

In principle, the macroscopic dissolution rate depends on several microscopic rates,  $r_i$ , as  $R = \sum r_i$ . Each  $r_i$  stems from different surface structures formed by organic ligands as well as a proton-promoted contribution. These microscopic dissolution rates depend on reactor conditions and hematite preparations. It is generally difficult to infer microscopic dissolution mechanisms solely from  $R$ . Even by varying reactor conditions to obtain several rates, the system is typically insufficiently constrained to determine the number and magnitude of microscopic rates. Some success has been achieved by asserting that no more than two microscopic pathways are available. For example, Furrer and Stumm (1986) assume that the macroscopic dissolution rate is composed of a proton-promoted and a ligand-promoted dissolution rate.

Another approach to determining microscopic rates utilizes direct spectroscopic evidence to determine the occurrence and concentration of specific surface complexes. We employ FTIR-ATR to determine the actual occurrence of the surface com-

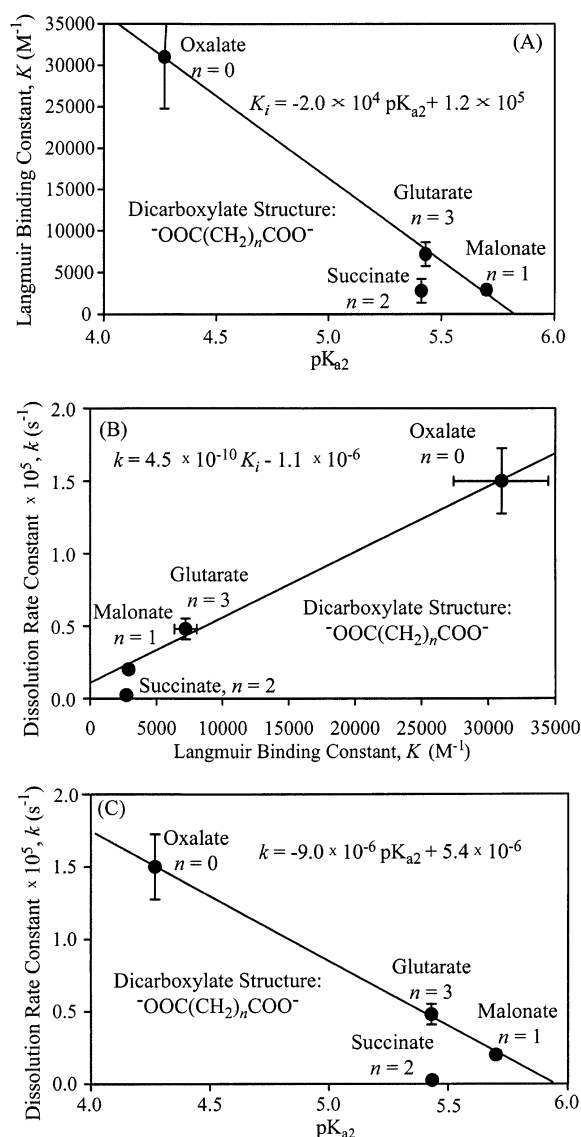


Fig. 12. Structure–activity correlations. (A) Model Langmuir binding constant ( $M^{-1}$ ) vs.  $pK_{a2}$ , (B) ligand-promoted dissolution rate constant ( $s^{-1}$ ) vs. Langmuir binding constant ( $M^{-1}$ ), and (C) ligand-promoted dissolution rate constant ( $s^{-1}$ ) vs.  $pK_{a2}$ . Correlations are for the ligands that form bidentate surface complexation structures (viz. oxalate, malonate, succinate, and glutarate). Acidity constants are from Martell and Smith (1977).

plexation structures proposed in Figure 1. Each of the structures C–F in Figure 1 should release iron from the surface at a different rate (i.e., structure-specific  $r_i$  values). Our spectroscopic data indicate that each ligand forms only one surface complexation structure at  $pH = 5.0$ , which corresponds to one ligand-promoted dissolution pathway. A proton-promoted rate is possible (Samson and Eggleston, 1998) but apparently negligible in our experiments, as determined in control studies (5 mM acetate, no dicarboxylate ligand) conducted at  $pH = 5.0$  where no dissolution was detectable. In addition to the suite of possible surface complexation structures (Fig. 1), additional complications arise from the possible micro-heterogeneity of

the hematite surface as well as the group of Miller-indexed faces terminating a three-dimensional crystal (Adamson and Gast, 1997). Each surface complexation structure on each face should have a characteristic microscopic dissolution rate constant, and each surface may have several types of sites (e.g., steps, kinks, or adatoms) not strictly accounted for in the depictions in Figure 1. However, we have no method to probe the heterogeneity of surface site energies and thus consider that the heterogeneity may be subsumed within an average surface site (Schindler and Stumm, 1987). By this approach, we are implicitly asserting that the surface complexation structures depicted in Figure 1 are quantitatively more important than the surface morphological features in the interpretation of the dissolution rates.

From these observations and assumptions, it follows that at the reactor conditions examined in this study, dissolution occurs by only one ligand-promoted pathway. With this understanding, we describe dissolution rate with the equation  $R = k\Gamma$ , where  $k$  is the first-order rate constant ( $s^{-1}$ ) and  $\Gamma$  is the ligand surface concentration ( $mol\ m^{-2}$ ). Surface charging, lateral interactions between adsorbates, differences in the atomic structure of different Miller index surfaces, and multiple adsorption sites all possibly affect the surface concentration. Omitting these complications, the total number of active sites ( $\Gamma_{\theta \rightarrow 1}$ ) is approximated from the number of iron atoms exposed in the (001) face of hematite. From the measured electronic structure of this face of hematite (Becker et al., 1996), we estimate the total site concentration as  $6.9 \times 10^{-6}\ mol\ m^{-2}$ . Our IR work shows  $\theta = 1$  for all ligands under the conditions of the dissolution experiments, i.e.,  $6.9 \times 10^{-6}\ mol\ m^{-2}$ . This surface concentration is consistent with several studies of the sorption of oxalate onto hematite at similar conditions (Zhang et al., 1985; Zinder et al., 1986; Banwart et al., 1989). Rate constants calculated with this surface concentration are shown in Table 2.

#### 4.6. Relationship between Surface Structures and Rates

Our interpretation of the IR spectroscopic data (section 4.3) indicates that each ligand forms only one surface complexation structure and that oxalate, malonate, and glutarate form bidentate surface structures (Fig. 1C or D). Figure 12B shows the correlation between the Langmuir binding constant calculated from the IR work and the microscopic dissolution rate constant (Table 2). Based on a linear least-squares fit, we offer the empirical generalization that ligands interacting with the hematite surface through two carboxylate groups promote dissolution as follows:

$$k = 4.5 \times 10^{-10} K - 1.1 \times 10^{-6} \quad (6)$$

Equation 6 states that the ligand-promoted dissolution rate constant is proportional to the adsorption strength of the ligand. The relationship is rationalized as follows. Strong interactions between the ligand and a surficial metal atom induce polarization of the bonds between the metal atom and the oxygen atoms in the mineral lattice. The polarization weakens the bond, thus lowering the energy barrier for the dissolution of metal atom. Figure 12C shows that there is also a linear relationship between the  $pK_{a2}$  value of the ligand and the microscopic dissolution rate constant, as follows:

$$k = -9.0 \times 10^{-6} \text{pK}_{a2} + 5.4 \times 10^{-6} \quad (7)$$

Equation 7 follows from the linear free energy relationship between the Langmuir binding constant of the bidentate ligands and their  $\text{pK}_{a2}$  values. Estimation of the ligand-promoted microscopic dissolution rate constants of other ligands that also form bidentate complexes is then possible from  $\text{pK}_{a2}$  values available in the literature (Martell and Smith, 1977).

Adipate and succinate form a monodentate complex with the surface iron atoms (Fig. 1E). The monodentate complex, having only one oxygen bond to the surface, donates less electron density to a surficial iron atom than the bidentate surface complexation structure, and thus the monodentate structure does not promote the dissolution of hematite. It is possible, though not determinable from our data, that the monodentate complex passivates the surface by occupying surface sites, effectively inhibiting other dissolution pathways (e.g., proton-promoted). Inhibition of dissolution has been indicated for other ligands such as sulfate, chromate, and benzoate (Stumm, 1992). In the current work, the magnitude rate of ligand-promoted hematite dissolution is in the order oxalate > malonate > succinate, which is consistent with the work of Furrer and Stumm (1986) on aluminum oxides. We attribute the slow rate of succinate-promoted dissolution to a monodentate structure based on the surface complexation structure assigned from infrared spectroscopy.

The monodentate structure (Fig. 1E) is similar to the bidentate binuclear structure (Fig. 1D) in that each oxygen bonds to only one surficial iron atom whereas in the bidentate mononuclear structure (C), two oxygens bind to a single iron atom. Because the electron polarization is similar in structures D and E, these structures should have similar dissolution rates. The IR work determines that oxalate, malonate, and glutarate bind as either C or D. Because we observe different dissolution rates for the monodentate and bidentate ligands, we infer that oxalate, malonate, and glutarate form bidentate mononuclear surface complexation structures (C) at  $\text{pH} = 5.0$ , as opposed to binuclear complexes (D). This conclusion is consistent with the findings of modeling studies of Mesuere and Fish (1992), who report a dominant bidentate mononuclear surface structure for oxalate on goethite at  $\text{pH} = 5.0$ . This assignment also agrees with the model proposed by Furrer and Stumm (1986) that ligands with one moiety do not strongly promote dissolution, whereas potential chelating ligands are capable of assisting dissolution.

In conclusion, we find that the studied ligands each form only one surface structure at  $\text{pH} = 5.0$ . Oxalate, malonate, and glutarate ( $n = 0, 1, \text{ and } 3$ ) form bidentate mononuclear surface complexation structures whereas succinate and adipate ( $n = 2 \text{ and } 4$ ) bind through one moiety. The absence of a correlation between  $n$  and the qualitative form of the surface structure is attributed to the propensities of the ligands to adopt geometrically favorable heterocyclic ring conformations. A linear free energy relationship is reported between the Langmuir binding constants estimated from the IR measurements and the  $\text{pK}_{a2}$  values of the chelating ligands. Dissolution rate constants correlate with ligand binding strength for bidentate structures formed by oxalate, glutarate, and malonate at  $\text{pH} = 5.0$ . Negligible dissolution occurs by monodentate structures formed by succinate and adipate at  $\text{pH} = 5.0$ , though these ligands do bind

strongly to the surface. We conclude that both the quantitative strength of the binding constant ( $K$ ) and the qualitative form of the surface complexation structure are important factors in the formulation of structure–activity relationships of ligand-promoted hematite dissolution. A linear free energy relationship is proposed between the dissolution rate constants of the bidentate ligands and both the  $\text{pK}_{a2}$  values and the Langmuir binding constants estimated from the IR measurements. The present work is a step towards the construction of a model for the prediction of the mobility of iron in natural systems.

*Acknowledgments*—Andrew Ghio (US EPA) graciously aided with the ICP-AES measurements. Jia Li and Peter Buseck (University of Arizona) kindly obtained the electron diffraction patterns. Daniel Albert (University of North Carolina) assisted in performing the BET surface area measurements. Laillah Rice contributed to the dissolution experiments as part of an undergraduate research project. Sherry Samson, Holly Chelf, Jeong-Ho Han, and Stephan Hug provided valuable discussion. OWD was funded by a United States Environmental Protection Agency Science to Achieve Results (USEPA STAR) Fellowship. The work described in this paper was completed during the authors' residence in the Department of Environmental Sciences and Engineering at the University of North Carolina at Chapel Hill.

*Associate editor:* G. Sposito

## REFERENCES

- Adamson A. W. and Gast A. P. (1997) *Physical Chemistry of Surfaces*. Wiley.
- Anderman M. and Kennedy J. H. (1988) Iron oxide ( $\text{Fe}_2\text{O}_3$ ). In *Semiconductor Electrodes* (ed. H. O. Finklea), pp. 153. Elsevier.
- Banwart S., Davies S., and Stumm W. (1989) The role of oxalate in accelerating the reductive dissolution of hematite ( $\alpha\text{-Fe}_2\text{O}_3$ ) by ascorbate. *Colloids and Surfaces* **39**, 303–309.
- Bargar J. R., Persson P., and Brown G. E. J. (1999) Outer-sphere adsorption of Pb(II)EDTA on goethite. *Geochim. Cosmochim. Acta* **63**, 2957–2969.
- Becker U., Hochella M. F. Jr., and Apra E. (1996) The electronic structure of hematite {001} surfaces: Applications to the interpretation of STM images and heterogeneous surface reactions. *American Mineralogist* **81**, 1301–1314.
- Benjamin M. M. (2000) Modeling bidentate adsorption: A. Return to the theater of the adsorb. *Proceedings of American Chemical Society National Meeting*.
- Bruno J. and Duro L. (2000) Reply to W. Hummel's comment on and correction to "On the Influence of Carbonate in Mineral Dissolution: I. The Thermodynamics and Kinetics of Hematite Dissolution in Bicarbonate Solutions at  $T = 25^\circ\text{C}$ " by J. Bruno, W. Stumm, P. Wersin, and F. Brandenberg. *Geochim. Cosmochim. Acta* **64**, 2173–2176.
- Bruno J., Stumm W., Wersin P., and Brandenberg F. (1992) On the influence of carbonate in mineral dissolution: I. The thermodynamics and kinetics of hematite dissolution in bicarbonate solutions at  $T = 25^\circ\text{C}$ . *Geochim. Cosmochim. Acta* **56**, 1139–1147.
- Cabaniss S. E., Leenheer J. A., and McVey I. F. (1998) Aqueous infrared carboxylate absorbances: Aliphatic di-acids. *Spectrochem. Acta A* **54**, 449–458.
- Carley A. F. and Morgan P. H. (1989) *Computational Methods in the Chemical Sciences*. Wiley.
- Carroll-Webb S. A. and Walther J. V. (1988) A surface complexation model for the pH-dependence of corundum and kaolinite dissolution rates. *Geochim. Cosmochim. Acta* **52**, 2609–2623.
- Collins C. R., Ragnarsdottir K. V., and Sherman D. M. (1999) Effect of inorganic and organic ligands on the mechanism of cadmium sorption to goethite. *Geochim. Cosmochim. Acta* **63**, 2898–3002.
- Cornell R. M., Posner A. M., and Quirk J. P. (1973) Crystal morphology and the dissolution of hematite. *J. Inorg. Nuc. Chem.* **36**, 1937–1946.
- Curl E. A. and Truelove B. (1986) *The Rhizosphere*. Springer-Verlag.

- Deacon G. B. and Phillips R. J. (1980) Relationships between the carbon-oxygen stretching frequencies of carboxylato-complexes and the type of carboxylate coordination. *Coord. Chem. Rev.* **33**, 227–250.
- Dobson K. and McQuillan A. (1999) In situ infrared spectroscopic analysis of the adsorption of aliphatic carboxylic acids to TiO<sub>2</sub>, ZrO<sub>2</sub>, Al<sub>2</sub>O<sub>3</sub>, and Ta<sub>2</sub>O<sub>5</sub> from aqueous solutions. *Spectrochim. Acta A* **55**, 1395–1405.
- Duckworth O. W. (2000) Ligand-promoted dissolution of hematite: Relationships between surface complexation structures and dissolution rate constants. M.S. thesis, University of North Carolina.
- Dzombak D. A. and Morel F. M. M. (1990) *Surface Complexation Modeling*. Wiley.
- Filius J. D., Heimstra T., and Van Riemsdijk W. H. (1997) Adsorption of small weak organic acids on goethite: Modeling of mechanisms. *J. Coll. Inter. Sci.* **195**, 368–380.
- Fujita J., Martell A. E., and Nakamoto K. (1962) Infrared spectra of metal chelate compounds. VII. Normal coordinate treatments on 1:2 and 1:3 oxalato complexes. *J. Chem. Phys.* **36**, 331–338.
- Furrer G. and Stumm W. (1986) The coordination chemistry of weathering: I. Dissolution kinetics of  $\delta$ -Al<sub>2</sub>O<sub>3</sub> and BeO. *Geochim. Cosmochim. Acta* **50**, 1847–1860.
- Greenberg A., Cleseri L., and Eaton A. (1992) *Standard Methods for the Examination of Water and Wastewater*. American Public Health Association.
- Hersman L., Lloyd T., and Sposito G. (1995) Siderophore-promoted dissolution of hematite. *Geochim. Cosmochim. Acta* **59**, 3327–3330.
- Huang W. H. and Keller W. D. (1971) Dissolution of clay minerals in dilute organic acids at room temperature. *Am. Min. Soc.* **56**, 1082–1095.
- Hug S. J. (1997) In situ Fourier transform infrared measurements of sulfate adsorption on hematite in aqueous solutions. *J. Colloid Inter. Sci.* **188**, 415–422.
- Hug S. J. and Sulzberger B. (1994) In situ Fourier transform infrared spectroscopic evidence for the formation of several different surface complexes of oxalate on TiO<sub>2</sub> in the aqueous phase. *Langmuir* **10**, 3587–3597.
- Jones D. (1998) Organic acids in the rhizosphere: A critical review. *Plant and Soil* **205**, 25–44.
- Kleinbaum D. G., Kupper L. L., and Muller K. E. (1988) *Applied Regression Analysis and Other Multivariable Methods*. Duxbury Press.
- Loundon G. M. (1988) *Organic Chemistry*. Benjamin/Cummings.
- Ludwig C., Devidal J., and Casey W. H. (1996) The effect of different functional groups on the ligand-promoted dissolution of NiO and other oxide minerals. *Geochim. Cosmochim. Acta* **60**, 213–224.
- March J. (1992) *Advanced Organic Chemistry*. Wiley.
- Martell A. E. and Smith R. M. (1977) *Critical Stability Constants*. Plenum Press.
- Martin S. T., Kesselman J. M., Park D. S., Lewis N. S., and Hoffmann M. R. (1996) Surface structures of 4-chlorocatechol adsorbed on titanium dioxide. *Environ. Sci. Technol.* **30**, 2535–2542.
- Maurice P. A., Hochella M. F. Jr., Parks G. A., Sposito G., and Schwertmann U. (1995) Evolution of hematite surface microtopography upon dissolution by simple organic acids. *Clays and Clay Minerals* **43**, 29–38.
- Mesuer K. and Fish W. (1992) Chromate and oxalate adsorption on goethite. I. Calibration of surface complexation models. *Environ. Sci. Technol.* **26**, 2357–2364.
- Miller W. P., Zelazny L. W., and Martins D. C. (1986) Dissolution of synthetic crystalline and noncrystalline iron oxides by organic acids. *Geoderma* **37**, 1–13.
- Nara M., Torii H., and Tasumi M. (1996) Correlation between the vibrational frequencies of the carboxylate group and the types of its coordination to a metal ion: An *ab initio* molecular orbital study. *J. Phys. Chem.* **100**, 19812–19817.
- Nordin J., Persson P., Laiti E., and Sjöberg S. (1997) Adsorption of *o*-phthalate at the water-boehmite ( $\gamma$ -AlOOH) interface: Evidence for two coordination modes. *Langmuir* **13**, 4085–4093.
- Parfitt R. L. and Farmer V. C. (1977) Adsorption on hydrous oxides I. Oxalate and benzoate on goethite. *J. Soil Sci.* **28**, 29–39.
- Rodenas L. A. G., Iglesias A. M., Weisz A. D., Morando P. J., and Blesa M. A. (1997) Surface complexation description of the dissolution of chromium(III) hydrous oxides by oxalic acids. *Inorg. Chem.* **36**, 6423–6430.
- Samson S. D. and Eggleston C. M. (1998) Active sites and the non-steady-state dissolution of hematite. *Environ. Sci. Technol.* **32**, 2871–2875.
- Schindler P. W. and Stumm W. (1987) The surface chemistry of oxides, hydroxides, and oxide minerals. In *Aquatic Surface Chemistry* (ed. W. Stumm), pp. 83–110. Wiley.
- Schnitzer M. and Kodama H. (1976) The dissolution of micas by fulvic acid. *Geoderma* **15**, 381–391.
- Schwertmann U. and Cornell R. M. (1991) *Iron Oxides in the Laboratory*. VCH Publishers.
- Stone A. T. (1987) Reductive dissolution of Mn(III/IV) oxides by substituted phenols. *Environ. Sci. Tech.* **21**, 979–988.
- Stone A. T. (1996) Reactions of extracellular organic ligands with dissolved metal ions and mineral surfaces. In *Geomicrobiology: Interactions between Microbes and Minerals*, Vol. 35 (eds. J. F. Banfield and K. H. Nielson). 309–349. Mineralogical Society of America.
- Stumm W. (1992) *Chemistry of the Solid–Water Interface*. Wiley.
- Stumm W. and Morgan J. J. (1996) *Aquatic Chemistry*. Wiley.
- Stumm W. and Wieland E. (1990) Dissolution of oxide and silicate minerals: Rates depend on surface speciation. In *Aquatic Chemical Kinetics* (ed. W. Stumm). 367–400. Wiley.
- Tejedor-Tejedor M. I. and Anderson M. A. (1986) “In situ” attenuated total reflection Fourier transform infrared studies of the goethite ( $\alpha$ -FeOOH)–aqueous solution interface. *Langmuir* **2**, 203–210.
- Tejedor-Tejedor M. I., Yost E., and Anderson M. A. (1990) Characterization of benzoic and phenolic complexes at the goethite/aqueous solution interface using cylindrical internal reflection Fourier transform infrared spectroscopy. Part I. Methodology. *Langmuir* **6**, 979.
- Wogelius R. A. and Walther J. V. (1991) Olivine dissolution at 25°C: Effects of pH, CO<sub>2</sub>, and organic acids. *Geochim. Cosmochim. Acta* **55**, 943–954.
- Zhang Y., Kallay N., and Matijevic E. (1985) Interactions of metal hydrous oxides with chelating agents. VII. Hematite–oxalic acid and –citric acid systems. *Langmuir* **1**, 201–206.
- Zinder B., Furrer G., and Stumm W. (1986) The coordination chemistry of weathering: II. Dissolution of Fe(III) oxides. *Geochim. Cosmochim. Acta* **50**, 1861–1869.